Sintering Hot Paper

Deutsche Ausgabe: DOI: 10.1002/ange.201605443
Internationale Ausgabe: DOI: 10.1002/anie.201605443

Cold Sintering: A Paradigm Shift for Processing and Integration of Ceramics

*Jing Guo[+], Hanzheng Guo[+], Amanda L. Baker, Michael T. Lanagan, Elizabeth R. Kupp, Gary L. Messing, and Clive A. Randall**

Abstract: *This paper describes a sintering technique for ceramics and ceramic-based composites, using water as a transient solvent to effect densification (i.e. sintering) at temperatures between room temperature and 200 °C. To emphasize the incredible reduction in sintering temperature relative to conventional thermal sintering this new approach is named the "Cold Sintering Process" (CSP). Basically CSP uses a transient aqueous environment to effect densification by a mediated dissolution–precipitation process. CSP of NaCl, alkali molybdates and V_2O_5 with small concentrations of water are described in detail, but the process is extended and demonstrated for a diverse range of chemistries (oxides, carbonates, bromides, fluorides, chlorides and phosphates), multiple crystal structures, and multimaterial applications. Furthermore, the properties of selected CSP samples are demonstrated to be essentially equivalent as samples made by conventional thermal sintering.*

Since the upper Paleolithic era mankind has fabricated ceramics with a high temperature process. The earliest archeological evidence of human manufacturing materials is the sintering of ceramics in the case of the iconic figurine, the Venus of Doli Vestonice.[1] We now generally regard most ceramics to be fabricated from powders and sintered between 50% and 75% of the melting temperature to >95% theoretical density. With high melting temperatures, most ceramics are sintered at >1000 °C.[2] Ceramic powders are increasingly integrated with metals, polymers or other ceramics to achieve improved properties and multifunctional devices.[3] Co-sintering of multimaterial systems is difficult due to the differences in thermal stability, shrinkage temperature onsets and rates, and the physical and chemical incompatibilities of the components at high temperatures.[4] The primary thermodynamic driving force for sintering is the reduction in surface free energy,[2a] and sintering mechanisms are classified as either solid state or liquid phase.[5] Many sintering process innovations increase the driving force for densification by applying pressures up to 200 MPa during the sintering process (e.g. hot pressing, hot isostatic pressing, and field assisted sintering (FAST)) or by enhancing diffusional processes with alternative, rapid volumetric heating strategies (e.g. microwave sintering, FAST, flash sintering)[6] that accelerate heating at the particle–particle level, but these processes still require high temperatures due to the slow solid state diffusional processes, or high temperature needed to form a liquid.

We demonstrate for the first time that a wide range of inorganic materials and ceramic-based composites can be sintered at much lower temperatures than previously thought possible by using either an acidic or basic aqueous solution as a low temperature solvent for the solution–precipitation process. There are a number of earlier contributions that indicate the advantage of using water to aid densification processes.[7] Our work demonstrates the use of small amounts of an aqueous solution to enhance densification across many different systems, and combinations of materials. To differentiate this process from conventional high temperature thermal sintering we name this sintering approach the "Cold Sintering Process (CSP)". To demonstrate the enormous potential and versatility of cold sintering, we present results for NaCl, alkali molybdates ($K_2Mo_2O_7$, $Na_2Mo_2O_7$, Li_2MoO_4) and V_2O_5, but we also foresee that new, non-obvious composite material systems can be perceived for the first time between organic and inorganic materials as a result of the ultralow temperatures of the CSP. A broad range of inorganic materials that have undergone densification under CSP (Table S1, Supporting Information) demonstrate the breath of material chemistries, crystal structures, and important technical ceramics with mechanical and multiple electrical functionalities possible by this approach.

Based on liquid phase sintering theory and our microstructure observations on a broad number of systems, a schematic illustration of the basic stages during CSP is shown in Figure 1 a. The ceramic powder is uniformly wetted with an appropriate amount of aqueous solution so that a liquid phase is intentionally introduced at the particle–particle interfaces. The dissolution of sharp edges of solid particles reduces the interfacial areas, aiding the rearrangement in the next sintering stage. Under appropriate pressure and temperature condition, the liquid phase redistributes itself and diffuses into the pores between the particles. The subsequent stage, often referred to as solution–precipitation, triggers a large chemical driving force for the solid and liquid phases to reach the equilibrium state. Under capillary

[*] Dr. J. Guo,[+] Dr. H. Guo,[+] A. L. Baker, Dr. E. R. Kupp, Prof. G. L. Messing, Prof. C. A. Randall
Materials Research Institute and Department of Materials Science & Engineering, The Pennsylvania State University
University Park, PA 16802 (USA)
E-mail: car4@psu.edu
Prof. M. T. Lanagan
Materials Research Institute, Department of Materials Science & Engineering and Department of Engineering Science & Mechanics, The Pennsylvania State University
University Park, PA 16802 (USA)
[+] These authors contributed equally to this work.

Supporting information for this article can be found under: http://dx.doi.org/10.1002/anie.201605443.

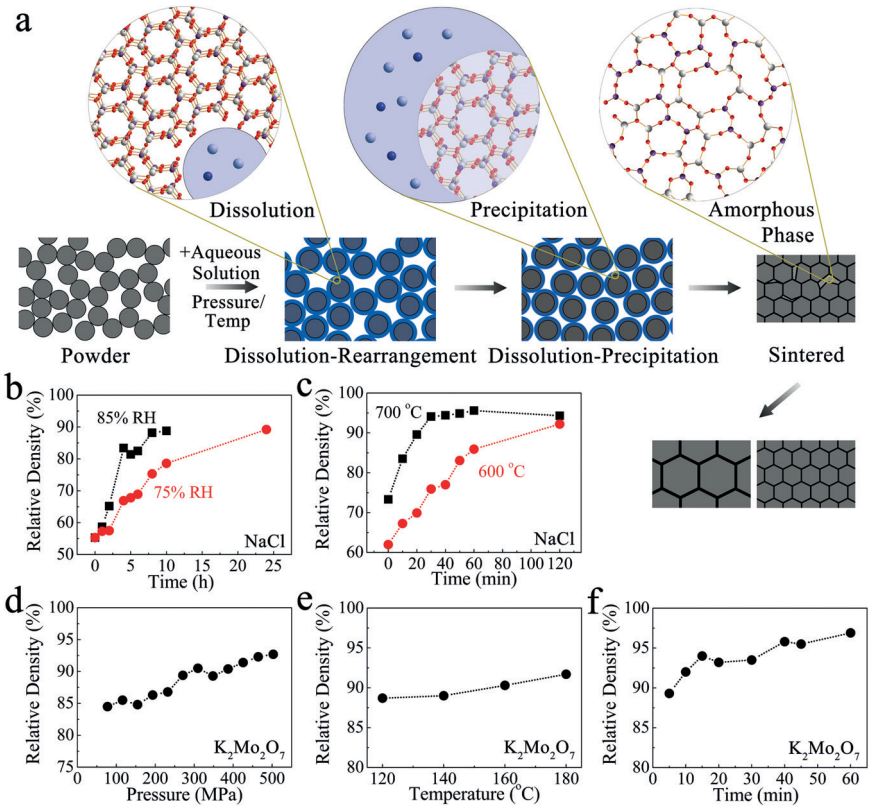

Figure 1. a) Schematic evolution of a powder compact during cold sintering. Interfaces at the grain boundary region in dominant stages have been magnified. Comparison of relative densities of ≈3 μm diameter NaCl under b) cold and c) conventional thermal sintering conditions. Relative densities of $K_2Mo_2O_7$ ceramics cold-sintered under controlled pressure, temperature, and isothermal holding time are displayed. d) At 120 °C for 5 minutes as a function of applied pressures. e) Under a pressure of 350 MPa for 5 minutes at various sintering temperatures. f) At 120 °C and 350 MPa as a function of isothermal holding time.

pressure, the contact areas between particles have a higher chemical potential, so that in this stage, ionic species and/or atomic clusters diffuse through the liquid and precipitate on particles at sites away from the stressed contact areas. The mass transport during this process minimizes the excess surface free energy of the compact and removes the porosity as the material forms a dense solid. In the final stage of sintering, an amorphous phase may form in some grain boundary areas; a process dependent on crystallography and solute speciation. The amorphous phase can suppress grain boundary diffusion or mobility, and thus limit grain growth. Elimination of water leaves an amorphous grain boundary phase which may or may not crystallize.

The data in Figure 1b shows the room temperature sintering kinetics of a 55% dense NaCl compact held at either 75% or 85% relative humidity (RH) for up to 24 h. We see that the salt samples densify from 55% to 69% in 5 h and to 90% relative density after 24 h in 75% RH air. The samples sintered at room temperature and 85% RH densify to 65% and 90% density after 2 h and 10 h, respectively. The microstructures of the 90% dense room temperature sintered NaCl consist of grains of approximately 20 to 30 μm in average size (Figure 2a,b). The grain growth is similar to that observed in many liquid phase thermally sintered ceramics as a result of the high solubility and long holding time. In Figure 1c we compare the densification kinetics of NaCl when thermally sintered at 600 °C and 700 °C. Even though these samples were heated at 600 °C and 700 °C they are only 84% dense after 50 min and 10 min, respectively. The microstructures show little grain growth relative to the initial NaCl powder (≈3 μm) as a result of the large amount of porosity (Figure 2c,d).

With high aqueous solubility at room temperature, salts like NaCl can easily densify with a small fraction of uniformly distributed water, thus demonstrating the power of the proper solvent for cold sintering. In the case of sparingly soluble materials, like ceramics, the cold sintering temperature and pressure are raised to enhance solubility and the process of densification.

Cold sintering of Li_2MoO_4, $Na_2Mo_2O_7$, $K_2Mo_2O_7$, and V_2O_5 illustrates the potential for sintering sparingly soluble single and mixed metal oxide ceramics. As shown in Figure 1d, $K_2Mo_2O_7$ samples are sintered to 80–85% relative density at 120 °C within 5 min under a pressure of 77 MPa. When the pressure is in the range of 270–390 MPa, the relative density of $K_2Mo_2O_7$ reaches 89%. Increasing sintering temperature from 120 °C to 180 °C (350 MPa for 5 min) cannot remarkably improve the relative density of $K_2Mo_2O_7$ (Figure 1e). But with holding time extended to 10–20 min (350 MPa and 120 °C), $K_2Mo_2O_7$ samples are sintered to 90–94% relative density (Figure 1f), which is comparable to those densities found with a conventional thermal sintering temperature of 460 °C. By appropriately varying temperature, pressure, holding time, and water chemistry and content, we cold sintered Li_2MoO_4, $Na_2Mo_2O_7$, $K_2Mo_2O_7$, and V_2O_5 samples to high density (>90%) ceramics at a temperature as low as 120 °C. The densities of cold-sintered Li_2MoO_4 (120 °C/ 350 MPa/ 15 min), $Na_2Mo_2O_7$ (120 °C/ 350 MPa/ 15 min), $K_2Mo_2O_7$ (120 °C/ 350 MPa/ 15 min), and V_2O_5 (120 °C/ 350 MPa/ 20 min) are 95.7%, 93.7%, 94.1% and 90.2%, respectively.

There are no obvious impurity or second phases after cold sintering (Figure S1, Supporting Information). As shown in Figure S2 (Supporting Information) and Figure 2e–j, the grain sizes of cold-sintered Li_2MoO_4, $Na_2Mo_2O_7$, $K_2Mo_2O_7$ ceramics are similar to the particle sizes of prepared Li_2MoO_4, $Na_2Mo_2O_7$, and $K_2Mo_2O_7$ powders, indicating that the grain growth is substantially limited under these experimental conditions. To this point, the grain sizes of the sintered ceramics could be easily tailored through control of the initial powder particle size. Such a technique may be utilized to

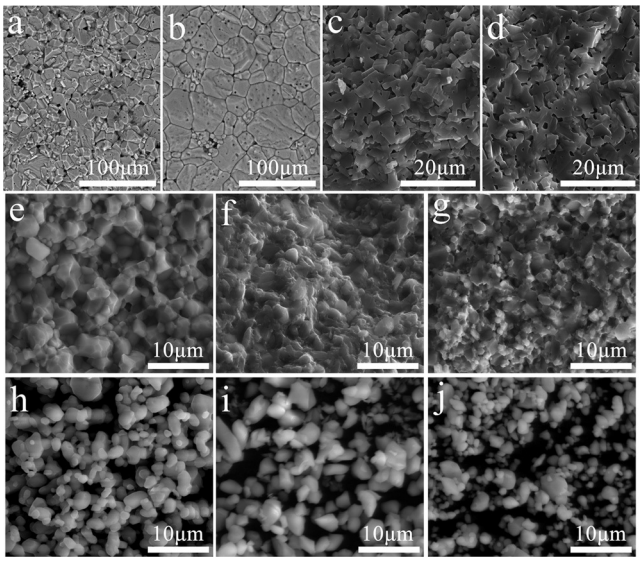

Figure 2. Microstructures of a–d) NaCl, e,h) Li_2MoO_4, f,i) $Na_2Mo_2O_7$, and g,j) $K_2Mo_2O_7$. NaCl sintered at a) room temperature and 75% relative humidity (RH) for 24 h, b) room temperature and 85% relative humidity for 10 h, c) 600 °C for 50 min, and d) 700 °C for 10 min. Cross-section of e) Li_2MoO_4, f) $Na_2Mo_2O_7$, and g) $K_2Mo_2O_7$ ceramics cold-sintered at 120 °C and 350 MPa for 15 min. Prepared h) Li_2MoO_4, i) $Na_2Mo_2O_7$, and j) $K_2Mo_2O_7$ powders.

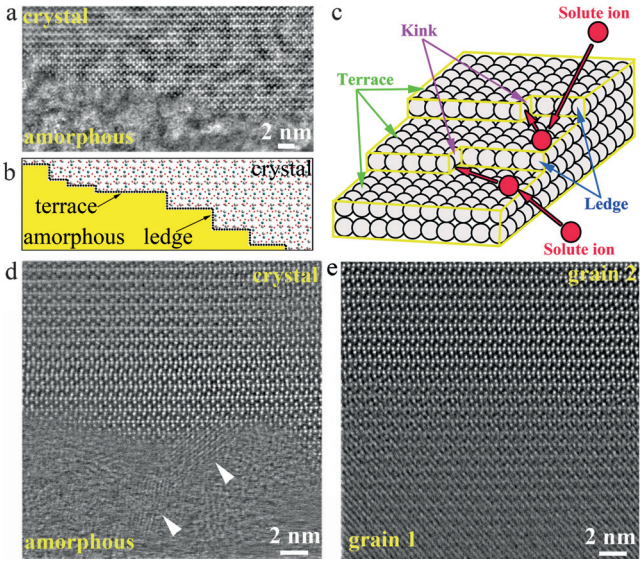

Figure 3. Interfaces of cold-sintered $Na_2Mo_2O_7$ ceramics and the Terrace–Ledge–Kink (TLK) model for crystal growth. a) HAADF-STEM image at the crystal/amorphous-phase interface. b) Schematic showing of the terraces and ledges. c) Schematic of the TLK model for crystal growth. d) HAADF-STEM image at the crystal/amorphous-phase interface with the appearance of nanometer-sized precipitates, as highlighted by the white triangles. e) HAADF-STEM image of the grain boundary. The bright-contrasted dots in (a), (d), and (e) are columns of Na atoms.

produce polycrystalline materials with controllable and uniform grain sizes, or even preserve the nanoscale size of the crystallites in the final products as shown in Figure S3c (Supporting Information). This set of experiments demonstrates the effective use of pressure to enhance the driving force for cold sintering. The pressure assists both particle rearrangement and the dissolution–precipitation process at particle contacts.

Since cold sintering involves precipitation of a complex metal oxide-based phase, the appearance of a small fraction of an amorphous phase in the ceramic grain boundaries seems reasonable (Figure S4, Supporting Information). The formation of an amorphous grain boundary phase depends on the rate of solute condensation as controlled by the rate of solvent evaporation, and the associated degree of solute supersaturation before condensation of the dissolved phase. We further studied the amorphous–ceramic interface in cold-sintered $Na_2Mo_2O_7$ from the atomic-scale view, with representative crystallites oriented along their [110] directions (Figure 3).

We observed that the amorphous–crystalline interface is typically arranged in a terrace-ledge manner (Figure 3b), which is consistent with the classic Terrace–Ledge–Kink (TLK) model[8] used to describe the equilibrium state of a growing crystal surface; the terrace ends in a ledge and steps down to another one, and the missing atoms in the ledge forms kink sites (Figure 3c). From a thermodynamic perspective, the step ledges and kinks provide energetically favorable sites for atomic diffusion and surface free energy minimization during liquid phase sintering, as the ionic species attached to these sites can establish a sufficient number of chemical bonds with the crystal surface so as to resist redissolving.[8c,9] Our EDS mapping results (Figure S5, Supporting Information) show that Na, Mo, and O homogeneously distributed across the crystalline/amorphous-phase interface region. This is also verified by further EDS quantification analysis performed for the corresponding region, which demonstrates a uniform chemical distribution without the notice of any significant deviation. In the amorphous phase, nanometer-sized precipitates are also observed to nucleate on the crystal surface (Figure 3d, as marked by the bright triangles). Additionally, we performed an extensive scanning/transmission electron microscopy (S/TEM) study to examine the grain–grain interface region in cold-sintered $Na_2Mo_2O_7$ ceramics. We estimate that 90% of grain boundaries have no amorphous phase, indicating that highly crystalline ceramics are approachable.

An additional proof of the utility and potential of cold sintering was found in the performances of cold-sintered NaCl, Li_2MoO_4, $Na_2Mo_2O_7$, $K_2Mo_2O_7$, and V_2O_5 ceramics, which are comparable to those prepared by conventional thermal sintering at 600–700 °C, 540 °C, 575 °C, 460 °C, and 450–660 °C, respectively (Table 1). The bonding of the room temperature sintered NaCl compact is similar to thermally sintered NaCl as illustrated by the comparable tensile strengths for samples ranging from 65 to 90% relative density (Figure S6, Supporting Information). The permittivities of cold-sintered Li_2MoO_4, $Na_2Mo_2O_7$, $K_2Mo_2O_7$ ceramics are similar to those of thermally sintered samples and the $Q \times f$ values are also good, as listed in Table 1. The DC conductivity of V_2O_5 ceramic is comparable to that of thermally sintered and hot-pressed[10] (630 °C/ 30–196 MPa) samples.

Table 1: Densities and performances of selected ceramics cold-sintered at room temperature without pressure (NaCl), or at 120 °C under a pressure of 350 MPa for 15–20 min (Li_2MoO_4, $Na_2Mo_2O_7$, $K_2Mo_2O_7$, and V_2O_5).

	Cold Sintering Process (CSP)		Conventional Thermal Sintering Process	
	Density [g cm^{-3}]	Performance[a]	Density [g cm^{-3}]	Performance
NaCl	1.95 (90%)	σ_s = 10–15 MPa	1.95–2.07 (90–95.6%)	σ_s = 7–21 MPa
Li_2MoO_4	2.9 (95.7%)	ε_r = 5.61 Q × f = 30500 GHz tanδ = 5.7 × 10^{-4} (f = 17.4 GHz)	2.895 (95.5%)	ε_r = 5.5 Q × f = 46000 GHz[11a]
$Na_2Mo_2O_7$	3.45 (93.7%)	ε_r = 13.4 Q × f = 14900 GHz tanδ = 7.5 × 10^{-4} (11.2 GHz)	3.59 (97%)	ε_r = 12.9 Q × f = 62400 GHz[11b]
$K_2Mo_2O_7$	3.39 (94.1%)	ε_r = 9.8 Q × f = 16000 GHz tanδ = 8.3 × 10^{-4} (13.3 GHz)		ε_r = 7.5 Q × f = 22000 GHz[11c]
V_2O_5	3.03 (90.2%)	σ_c = 4.8 × 10^{-4} S cm^{-1}		σ_c = 10^{-5}–10^{-3} S cm^{-1}[11d–f]

[a] σ_s, tensile strength. ε_r, microwave permittivity. tanδ, loss. Q, quality factor (Q = 1/tanδ). f, resonate frequency. σ_c, DC conductivity.

To date, we have shown that many simple and mixed metal oxides, metal chlorides and composites with a number of crystal structures and melting temperatures can be sintered between room temperature and 200 °C, as listed in Table S1 (Supporting Information). It should be noted that under CSP there are important and subtle process conditions that may vary to enable high densification of the materials listed in Table S1. The specific details will be addressed in future publications.

CSP draws on a diverse and multidisciplinary range of specializations including aqueous thermodynamics, chemical weathering, hydrothermal crystal growth, and biomineralization.[12] The low energy needed to densify the ceramics under the CSP is indicative of a non-equilibrium process involving surface reactions, which require an open system and changes in the chemical potential at the interfaces. The kinetics of the process can be dependent on crystal structure, surface area of the particles, pH of the solvent, the stoichiometry of the dissolution products, temperature, time and pressure. There are, of course, many details and challenges that need to be understood to establish the scientific foundations and ultimate control of CSP, in particular, understanding the diffusion processes under the transient evaporation of the water in and around the interfaces of the particle ensemble. As summarized in Figure S3 (Supporting Information), there are many new opportunities for the integration of different materials at these low temperatures that are non-obvious based on the previous practice of sintering inorganic particles at high temperatures. In summary, we regard the cold sintering process and its applicability across a number of crystal structures and compositions as an important contribution to ceramic processing and manufacturing. CPS offers the potential for a strategic revolution that could alter the material selections, improve performance, and expand integration options in material device applications and additive manufacturing.

Experimental Section

Cold sintering of NaCl**:** The NaCl powders were uniaxially pressed in a 12.5 mm steel die at 5 MPa to produce 55% dense samples that were stored in a desiccator prior to sintering studies. For room temperature (25 °C) sintering, samples were placed in a constant relative humidity chamber containing either supersaturated NaCl or KCl solutions to obtain a constant relative humidity of 75% or 85%, respectively.[13] Samples were held for up to 24 h and then the relative densities were calculated from sample dimensions after drying. Samples gained very little weight (< 0.2 wt.%) for up to 15 and 10 h, respectively. Samples were also thermally sintered by heating in air at 5 °C min^{-1} up to 600 °C and 700 °C and held for up to 2 h.

Bulk ceramic preparation**:** Dense ceramics of Li_2MoO_4, $Na_2Mo_2O_7$, $K_2Mo_2O_7$, and V_2O_5 and dense composites of 0.8 Li_2MoO_4-0.2 $BaFe_{12}O_{19}$, 0.5 Li_2MoO_4-0.5 PTFE, and 0.8 Li_2MoO_4-0.2 EG were prepared by cold sintering. Method 1: All the powders were mixed with 4–25 wt.% deionized water using a mortar and pestle. The moistened powders were uniaxially warm pressed in a steel die into dense pellets (12.7 mm in diameter and 1–5 mm in height) at 80–570 MPa and 120 °C. The die was preheated to 120 °C for more than 1 h. After cold sintering the pellets were placed into an oven at 120 °C for 6 h to remove water. Method 2: All the dry powders were pressed into pellets (12.7 mm in diameter and 1–5 mm in height) at 30–70 MPa at room temperature. Then, the pellets were stored in a constant relative humidity (water vapor generated by heating deionized water or humidity chamber) for 10–360 min. Finally, the moistened pellets were warm pressed with a steel die into dense pellets at 80–570 MPa and 120 °C and placed into an oven at 120 °C for 6–12 h to dry the samples.

The experimental details of powder preparation, multilayer ceramic preparation, and characterization are available in the Supporting Information.

Acknowledgements

H.G. would like to thank Dr. K. Wang (Materials Characterization Lab, The Pennsylvania State University) for his help and discussion on the electron microscopy work. J.G. and A.B. would like to thank L. Gao (Materials Research Institute, The Pennsylvania State University) for tape casting advice with QPAC. The authors would like to acknowledge financial support from the National Science Foundation, as part of the Center for Dielectrics and Piezoelectrics under Grant Nos. IIP-1361571 and 1361503.

Keywords: ceramics · cold sintering · composites · hydrothermal synthesis · sintering

How to cite: *Angew. Chem. Int. Ed.* **2016**, *55*, 11457 – 11461
Angew. Chem. **2016**, *128*, 11629 – 11633

[1] P. B. Vandiver, O. Soffer, B. Klima, J. Svoboda, *Science* **1989**, *246*, 1002 – 1008.
[2] a) M. N. Rahaman, *Sintering of Ceramics*, CRC Press, Boca Raton, **2008**; b) I. W. Chen, A. Rosenflanz, *Nature* **1997**, *389*, 701 – 704; c) Z. J. Shen, Z. Zhao, H. Peng, M. Nygren, *Nature* **2002**, *417*, 266 – 269; d) H. Shimizu, H. Z. Guo, S. E. Reyes-Lillo, Y. Mizuno, K. M. Rabe, C. A. Randall, *Dalton Trans.* **2015**, *44*, 10763 – 10772.
[3] a) B. L. Smith, T. E. Schäffer, M. Viani, J. B. Thompson, N. A. Frederick, J. Kindt, A. Belcher, G. D. Stucky, D. E. Morse, P. K. Hansma, *Nature* **1999**, *399*, 761 – 763; b) C. W. Nan, M. I. Bichurin, S. X. Dong, D. Viehland, G. Srinivasan, *J. Appl. Phys.* **2008**, *103*, 031101; c) M. T. Sebastian, H. Jantunen, *Int. J. Appl. Ceram. Technol.* **2010**, *7*, 415 – 434; d) B. T. McGrail, A. Sehirlioglu, E. Pentzer, *Angew. Chem. Int. Ed.* **2015**, *54*, 1710 – 1723; *Angew. Chem.* **2015**, *127*, 1730 – 1743; e) A. Mattern, B. Huchler, D. Staudenecker, R. Oberacker, A. Nagel, M. J. Hoffmann, *J. Eur. Ceram. Soc.* **2004**, *24*, 3399 – 3408; f) J. Guo, D. Zhou, H. Wang, Y. H. Chen, Y. Zeng, F. Xiang, Y. Wu, X. Yao, *J. Am. Ceram. Soc.* **2012**, *95*, 232 – 237; g) P. Barpanda, J. N. Chotard, C. Delacourt, M. Reynaud, Y. Filinchuk, M. Armand, M. Deschamps, J. M. Tarascon, *Angew. Chem. Int. Ed.* **2011**, *50*, 2526 – 2531; *Angew. Chem.* **2011**, *123*, 2574 – 2579.
[4] a) A. Mohanram, S. H. Lee, G. L. Messing, D. J. Green, *J. Am. Ceram. Soc.* **2006**, *89*, 1923 – 1929; b) D. J. Green, O. Guillon, J. Rödel, *J. Eur. Ceram. Soc.* **2008**, *28*, 1451 – 1466.
[5] a) W. D. Kingery, *J. Appl. Phys.* **1959**, *30*, 301 – 306; b) O. H. Kwon, G. L. Messing, *J. Am. Ceram. Soc.* **1990**, *73*, 275 – 281; c) S. J. L. Kang, *Sintering: Densification, Grain Growth and Microstructures*, Elsevier, Oxford, **2004**.
[6] a) R. Roy, D. Agarwal, J. P. Chen, S. Gedevanishvili, *Nature* **1999**, *399*, 668 – 670; b) U. Anselmi-Tamburini, J. E. Garay, Z. A. Munir, *Scr. Mater.* **2006**, *54*, 823 – 828; c) M. Cologna, B. Rashkova, R. Raj, *J. Am. Ceram. Soc.* **2010**, *93*, 3556 – 3559.
[7] a) C. A. Randall, J. Guo, H. Guo, A. Baker, M. T. Lanagan, *US Provisional Patent Application* 62/234,389, **2015**; b) S. Sōmiya, *Mater. Res. Soc. Symp. Proc.* **1984**, *24*, 255 – 271; c) H. Kähäri, M. Teirikangas, J. Juuti, H. Jantunen, *J. Am. Ceram. Soc.* **2014**, *97*, 3378 – 3379.
[8] a) I. N. Stranski, *Z. Phys. Chem.* **1928**, *136*, 259 – 278; b) W. Kossel, *Nachr. Ges. Wiss. Goettingen Math.-Phys. Kl.* **1927**, 135; c) A. E. Nielsen, *Kinetics of Precipitation*, Pergamon, Oxford, **1964**.
[9] S. J. L. Kang, M. G. Lee, S. M. An, *J. Am. Ceram. Soc.* **2009**, *92*, 1464 – 1471.
[10] K. Honma, M. Yoshinaka, K. Hirota, O. Yamaguchi, J. Asai, Y. Makiyama, *Mater. Res. Bull.* **1996**, *31*, 531.
[11] a) D. Zhou, C. A. Randall, H. Wang, L. X. Pang, X. Yao, *J. Am. Ceram. Soc.* **2010**, *93*, 1096 – 1100; b) G. Q. Zhang, H. Wang, J. Guo, L. He, D. D. Wei, Q. B. Yuan, *J. Am. Ceram. Soc.* **2015**, *98*, 528 – 533; c) G. Q. Zhang, J. Guo, L. He, D. Zhou, H. Wang, J. Koruza, M. Kosec, *J. Am. Ceram. Soc.* **2014**, *97*, 241 – 245; d) D. K. Chakrabarty, D. Guha, A. B. Biswas, *J. Mater. Sci.* **1976**, *11*, 1347 – 1353; e) I. H. Ismailzade, A. I. Alecberov, R. M. Ismailov, I. M. Aliyez, D. A. Rzayev, *Ferroelectrics* **1980**, *23*, 47 – 49; f) T. Nenov, Z. Nenova, *Proc. 23rd Int. Conf. Microelectron.* **2002**, *1*, 257 – 260.
[12] a) H. W. Nesbitt, G. M. Bancroft, W. S. Fyfe, S. N. Karkhanis, A. Nishijima, *Nature* **1981**, *289*, 358 – 362; b) Y. Chen, S. L. Brantley, *Chem. Geol.* **1997**, *135*, 275 – 290; c) W. Stumm, R. Wollast, *Rev. Geophys.* **1990**, *28*, 53 – 69; d) R. W. Revie, H. H. Uhlig, *Uhlig's Corrosion Handbook*, Wiley, Hoboken, **2011**; e) J. Hulliger, *Angew. Chem. Int. Ed. Engl.* **1994**, *33*, 143 – 162; *Angew. Chem.* **1994**, *106*, 151 – 171; f) D. E. Bugaris, H. C. zur Loye, *Angew. Chem. Int. Ed.* **2012**, *51*, 3780 – 3811; *Angew. Chem.* **2012**, *124*, 3844 – 3876; g) S. Weiner, L. Addadi in *Annu. Rev. Mater. Res.*, *Vol. 41* (Eds.: D. R. Clarke, P. Fratzl), Annual Reviews, Palo Alto, **2011**, pp. 21 – 40.
[13] L. Greenspan, *J. Res. Natl. Bur. Stand. Sect. A* **1977**, *81*, 89 – 96.

Received: June 3, 2016
Revised: July 15, 2016
Published online: August 11, 2016

